Research Article

A drastic change in glacial dynamics at the beginning of the seventeenth century on Novaya Zemlya coincides in time with the strongest volcanic eruption in Peru and the Great Famine in Russia

Valeriy Rusakov* (ORCID), Tat'yana Kuz'mina, Alexander Borisov, Irina Gromyak, Denis Dogadkin, Tat'yana Romashova, Galina Solovi'eva and Ruslan Lukmanov

Vernadsky Institute of Geochemistry and Analytical Chemistry (GEOKHI), Russian Academy of Sciences, Kosygina 19, 119991 Moscow, Russia

Abstract

In this study, we reconstructed for the first time the recent 1000-yr-long history of Goluboi tidewater glacier at the eastern side of the Novaya Zemlya, Kara Sea, based on accelerator mass spectrometry ^{14}C dating with higher-resolution age control on the basis of ^{210}Pb and ^{137}Cs radionuclides for the time period after AD 1885, using multiproxy analyses (lithology, mineralogy, and geochemistry) of proximal glaciomarine sediments from the Oga Fjord. Against the background of the active glacial dynamics and the intense meltwater runoff until the end of the sixteenth century, there was a sudden cooling at the beginning of the seventeenth century, which manifested itself in a significant decrease in the sedimentation rates. In time, this event coincides with the strongest volcanic eruption, AD 1600, in South America (in Peru) in the history of human settlement of the continent, which may have plunged the globe into cold climate chaos (Witze, 2008), and caused the Great Famine, AD 1601 to AD 1603, in Russia. The synchronicity of the described events may be an additional fact confirming the global impact of the eruption on the climate of our planet.

Keywords: Proximal glaciomarine sediments, tidewater glacier, fjord, Novaya Zemlya, last millennium

(Received 13 September 2021; accepted 17 December 2021)

INTRODUCTION

To understand the ongoing drastic changes in the Arctic (e.g., Meeker and Mayewski, 2002; Isaksson et al., 2005; Miller et al., 2010; Divine et al., 2011; Spielhagen et al., 2011; Trouet et al., 2009, 2012; Jernas et al., 2013; Opel et al., 2013; Luoto and Nevalainen, 2015; Serreze and Stroeve, 2015; Pawłowska et al., 2016; Polyakov et al., 2017; Linderholm et al., 2018; Nicolle et al., 2018; Werner et al., 2018), more accurate and high-resolution data about past environmental changes in the region are required. The data can be provided by sediment records from specific local regions having high sedimentation rates. These regions include the northern fjords of Novaya Zemlya archipelago (hereafter Novaya Zemlya) with internal deepwater basins that, without hiatuses, serve as natural reservoirs for continuous sediment accumulation (Murdmaa et al., 2004; Polyak et al., 2004).

The main source of glaciomarine sedimentary material in the fjords is suspension-rich glacial meltwater and terrestrial materials of various sizes supplied by icebergs and sea ice (Syvitski, 1989).

In fjords, the changes in lithology and the variations in the mineral and chemical composition of glaciomarine sediments are determined by glacial dynamics. In turn, the glacial dynamics are controlled by internal (such as subglacial drainage systems and internal stresses) and external (such as climate and glacial mass-balance conditions) glaciological factors (e.g., Meier and Post, 1969; Clarke, 1987; Eisen et al., 2001; Copland et al., 2003; Nesje and Dahl, 2003; Matthews and Briffa, 2005), as well as geomorphological factors (such as length and area; e.g., Evans and Rea, 2003; Ottesen and Dowdeswell, 2006; Ottesen et al., 2008). Meanwhile, the dynamics of the Novaya Zemlya glaciers and the climate variability in the region are quite complex and far from being fully understood (e.g., Shumskii, 1949; Chizhov et al., 1968; Zeeberg and Forman, 2001; Moore, 2013; Carr et al., 2014; Melkonian et al., 2016).

There are only two publications (Murdmaa et al., 2004; Polyak et al., 2004) devoted to the recent paleoenvironmental evolution of the northern Novaya Zemlya fjords that present lithologic, microfossil, and isotope records of the 6-m-long core ASV-987 from the Russkaya Gavan' Fjord located on its west coast. According to accelerator mass spectrometry (AMS) ^{14}C radiocarbon dating of benthic foraminifera found in the core, the core spans approximately 800 yr. The authors conclude that the glaciers on the west coast of Novaya Zemlya are sensitive to regional and global climatic changes. Currently, there are no publications on similar paleoreconstructions with respect to the records from glaciomarine sediment sequences of the eastern Novaya Zemlya fjords.

Our study fills the gap in the existing literature and presents a 1000-yr-long history of environmental changes in the eastern fjord of Novaya Zemlya (the least explored area of the Arctic) reconstructed through a multiproxy-based study, the AMS ^{14}C, and the short-lived radionuclide dating of sediment core AMK-5248. In addition to the lithologic description, grain-size analysis, ice, and iceberg-rafted debris (IRD), we analyze the mineral and chemical composition, including rare earth elements (REE), of the sediments found in the core. The data on grain-size and chemical composition were processed by mathematical statistics methods, which revealed certain small-scale variability of sedimentation environments superimposed on general trends in climate-driven environmental changes.

PHYSIOGRAPHIC AND OCEANOGRAPHIC SETTING

Glaciers of the northern Novaya Zemlya represent remnants of the last late Pleistocene ice sheet that occupied the Barents Sea (e.g., Gataullin et al., 1993, 2001; Polyak and Solheim, 1994; Polyak et al., 1995, 1997, 2000; Zeeberg et al., 2001; Svendsen et al., 2004; Hughes et al., 2015; Patton et al., 2015; Batchelor et al., 2019). In this region, postglacial warming and sea-level rise that began at ~20 to 19 ka BP (Fairbanks 1989; Yokoyama et al., 2000; Mix et al., 2001; Clark et al., 2009; Carlson and Clark, 2012; Lambeck et al., 2014) initiated an inland frontal retreat of the glaciers and flooding of the deep and extended fjords behind them. The Oga Fjord, with a maximum water depth of 190 m, is separated from the Novaya Zemlya Trough by an almost vertical sill (top of the sill <50 m water depth), featuring a chain of small islands, and consists of three local deepwater basins (Fig. 1). The site of the studied core is located in the inner basin, adjacent to the Goluboi tidewater glacier that serves as a natural trap for proximal glaciomarine sediments.

Extensive valleys that crosscut the North Island in the latitudinal direction from the Barents Sea to the Kara Sea serve as natural channels for glaciers; the Goluboi glacier originated from the main ice cap of the island (Kotlyakov, 1978). According to Chizhov et al. (1968), the valleys are cut almost perpendicularly by bedrock ridges stretching from north to south. At the intersection with the valleys, the ridges form narrow barriers. The shallow sill in the Oga Fjord (Fig. 1d) represents a similar barrier composed of rocks resistant to denudation.

Oceanographic studies in the northern fjords on the east coast of Novaya Zemlya revealed a seasonal pycnocline (at water depths of 10–15 m) separating the surface water layer (<30‰) and underlying seawater (>34‰; Korsun and Hald, 1998). Similar vertical salinity profiles are also typical for the Oga Fjord. However, here they are distinguished by a thicker (25–30 m) upper layer (24–32‰; Udalov et al., 2019), which indicates a stronger influence of glacial meltwater runoff. The pronounced water stratification causes the development of an estuarine-type circulation in the fjord, wherein the meltwater discharge leads to an increase in the counterflow of open-sea waters (Howe et al., 2019). Isotopic studies of the waters in eastern fjords (Kossova et al., 2019) showed that the water layer above the halocline contains up to 30% of the freshwater component, formed from a mixture of local glacial meltwater and waters of the Ob' River's runoff. The Ob' River's runoff waters are brought to the eastern fjords of the archipelago by the Eastern Novaya Zemlya Current (Gorshkov, 1980).

MATERIALS AND METHODS

Core AMK-5248 was retrieved at a site with coordinates 74° 37.9′N, 59°18.3′E and a water depth of 129 m during the 63rd cruise of RV *Akademik Mstislav Keldysh* in 2015 (Fig. 1c). Core sampling was carried out by means of a box corer and a gravity corer; the total length of the sections was 26 cm and 402 cm, respectively (Fig. 2). Because the gravity corer destroys the uppermost soft sediment layer, the studied sedimentary sequence is a combination of the two cores, correlated based on the down-core variability in water content, grain size, and chemical composition. It was found that the lower boundary of the upper sediment layer destroyed by the gravity corer corresponds to 19 cm (Fig. 2).

Activity of natural (^{210}Pb) and technogenic (^{137}Cs) radionuclides was continuously (every 2 cm) measured in the box core section. The samples were measured on a low-background gamma-spectrometric complex having multilayer passive shielding (lead, old low-background iron, copper, and plexiglass). For recording purposes, we used a BEGe3825 broadband detector made of ultrapure germanium of the planar type (Canberra, USA) having a thin carbon composite entrance window (0.6 mm wide), crystal diameter of 70 mm, an area of 3800 mm^2, and a thickness of 25 mm, which makes it possible to record gamma quanta with energies from 5 keV to 3 MeV. Notably, the energy resolution along the 1332 keV ^{60}Co line was not less than 1.7 keV and that along the ^{57}Co 122 keV isotope line was not less than 0.6 keV. The collection and processing of information was carried out on a DSA-1000 pulse analyzer (Canberra, USA). DSA-1000 is a complete integrated multichannel analyzer with 16 channels, built with reference to modern digital signal processing technology. In combination with the DSA-1000 analyzer (connected to a computer), the BEGe3825 germanium detector forms a complete spectrometric unit, providing the highest-quality collection and analysis of spectra. In this study, Genie 2000 v. 3.2.1 software was used to analyze the spectrum obtained on the detector. The results are summarized in Table 1.

The dating model used in this study was based on four AMS ^{14}C dating results of benthic foraminifera; these results were obtained from the Poznań Radiocarbon Laboratory (Fig. 2, Table 2). The choice of intervals for dating the benthic foraminifera was determined by the availability of a sufficient number of tests (>0.7 mgC). In the upper part of the box core, the required number of foraminifera was collected from several samples in the 6–12 cm interval. AMS ^{14}C dating was calibrated to calendar years using the Calib Rev v. 8.1.0 software (www.calib.org) with the 402 yr standard reservoir correction provided by the program and the Marine20 calibration database, assuming the age of the surface sample to be the year of core sampling, AD 2015 (Supplementary Table 1).

After onboard lithologic description of the core, the "wet" samples taken in plastic bags were stored at a temperature of ~0°C until they were transported to onshore laboratories. Parts of individual samples were dried to determine their water content. Water content was determined as the weight difference between the wet and dry samples (Supplementary Table 2).

Grain-size analysis was carried out with wet samples using the wet-sieve and decantation method, as proposed by Petelin (1967) and later improved by Andreeva and Lapina (1998). Before sieve dispersion and decantation, the wet samples were dispersed using ultrasound in an ultrasonic bath for 5 min at a vibration frequency of 21–22 kHz. To calculate the content of fine silt and clay fractions (<0.01 mm), the specific gravity of the average sample was taken as 2.55 g/cm^3. The sedimentation rate of the fine particles in the water column and the time for pouring the suspension out of the cans were calculated using the Stokes law and Arkhangelsky formulas (coefficients 2/9 and 0.16, respectively).
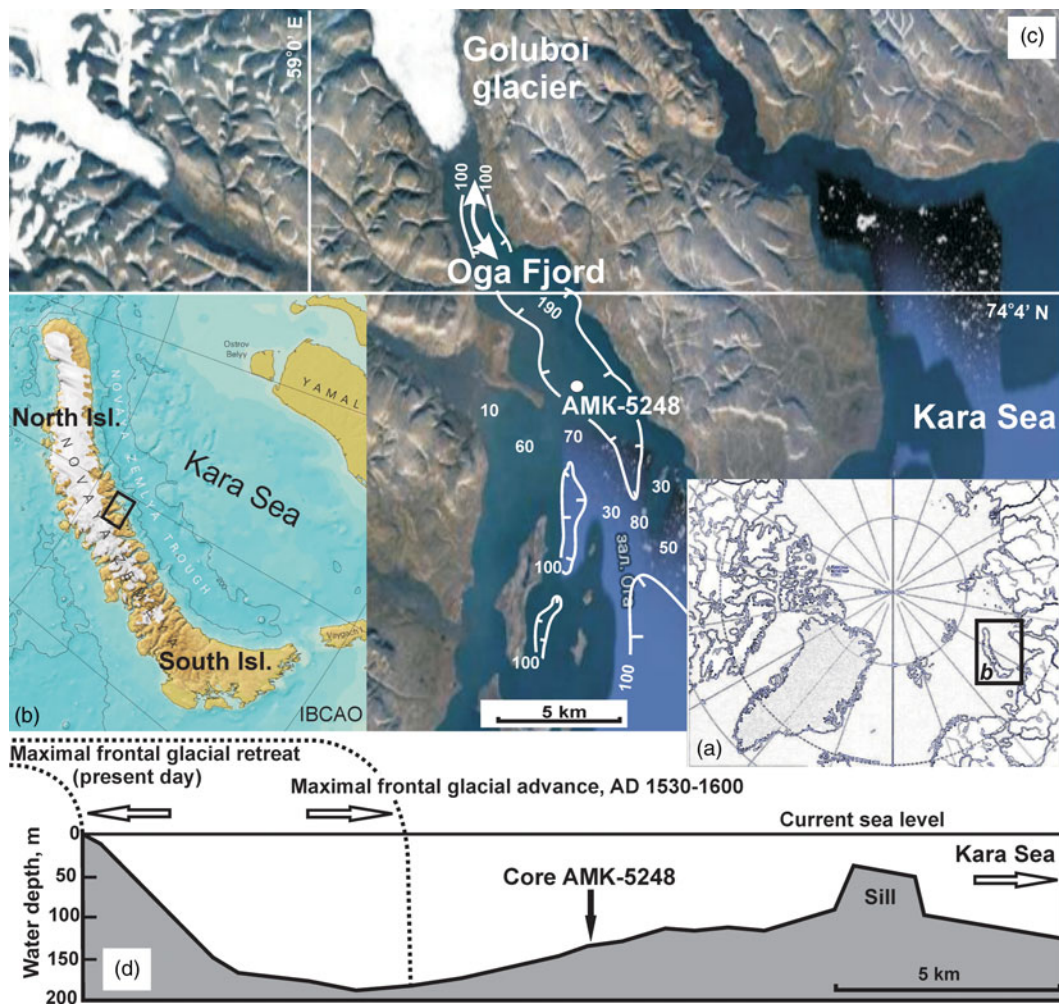
Figure 1. Overview map of the Arctic Ocean, the Novaya Zemlya archipelago, and the study area: (a) the Arctic Ocean; (b) Novaya Zemlya, the solid box outlines index map in c; (c) satellite image of the Oga Fjord fed by the Goluboi tidewater glacier and the position of core AMK-5248 (100 m isobath is drawn in white lines, separate numbers show water depths, white arrows indicate the most likely direction of the frontal glacial movement in the past); (d) water depth profile along the Oga Fjord and site of core sampling is shown on the profile, along with the glacial fronts currently and during AD 1530 to AD 1600 (dotted lines).

The size of the sieves corresponds to the selected fractions >0.01 mm in Supplementary Table 2. The grain-size data are summarized in Supplementary Table 2.

The mineral composition of several dried samples was studied using an X-ray diffractometer (XRD). The X-ray diffraction patterns from the samples were obtained using the Ultima-IV XRD (Rigaku, Japan) and semiconductor 1D detector D/Tex Ultra, (scan range of 3–65°2θ, scan speed of 3°2θ/min, and step of −0.02°2θ). The mineralogical composition was analyzed via the method applied by Moore and Reynolds (1997); the quantitative composition of the samples was estimated by applying the Rietveld method (Post and Bish, 1989) using the BGMN code (Profex software v. 3.14.3; Doebelin and Kleeberg, 2015). The results are summarized in Supplementary Table 3.

For chemical composition analysis, sediment was dried at temperatures of up to +105 °C. No washing of sea salt was done to avoid the loss of elements due to desorption and solubility in freshwater. Chemical composition was studied using two methods: X-ray fluorescence (XRF) and inductively coupled plasma atomic emission spectrometry (ICP-AES). XRF analysis was carried out on a stationary spectrometer, with a scanning channel AXIOS Advanced (PANalytical BV, Netherlands), which has an X-ray tube (with a rhodium anode as a source of excitation of characteristic radiation). We used 36 standard samples of bottom sediments, soils, and rocks to calibrate the spectrometer, obtain the characteristics of the calibration curves, and quantify the rock-forming oxides and impurity elements in the samples. The content of the following elements was determined: Si, Al, Ti, Fe, Mn, K, Ca, Mg, Na, P, Cr, S, V, Co, Ni, Cu, Zn, Rb, Sr, Nb, Pb, Zr, Ba, and Y, as well as loss on ignition (Supplementary Table 4). ICP-AES was performed on the ICAP-6500 Duo plasma Echelle spectrometer (Thermo Scientific, UK). The emission spectral range of 166–847 nm was recorded on a highly sensitive semiconductor detector charge-injection device. The REE and yttrium content (collectively "REY") determined is given in Supplementary Table 5.

The data on grain-size and chemical composition were processed by mathematical statistics methods using the standard Statgraphics Plus v. 10 software package. To assess the degree of heterogeneity of the studied samples, methods of statistical analysis such as factor analysis in the R-modification were applied.
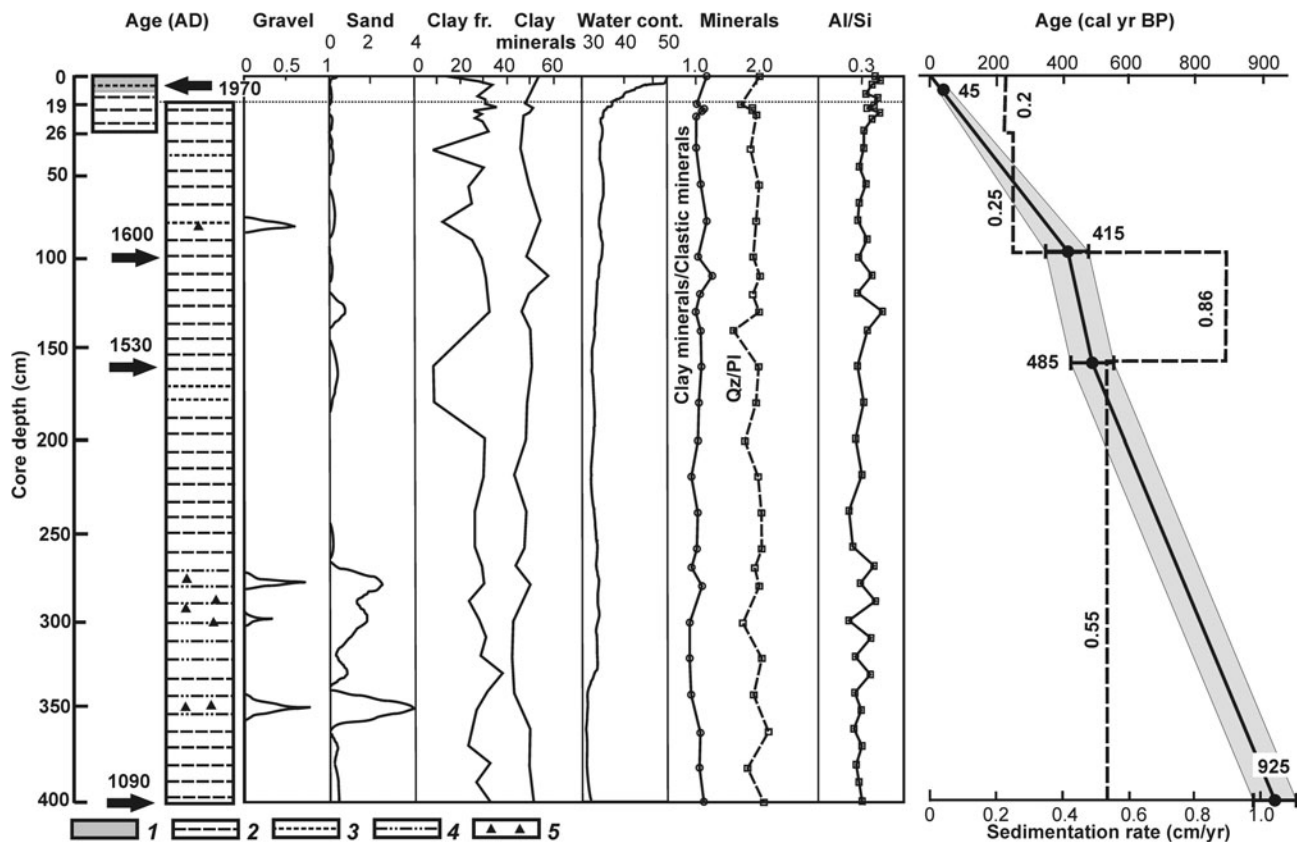
Figure 2. Lithologic scheme of core AMK-5248, built on the basis of a preliminary (field) description, as well as grain-size analysis (Supplementary Table 2): 1, watered sludge with a water content of 40–50 wt%; 2, clayey silt; 3, silt; 4, clayey silt with thin (<1 cm) sand interlayers; and 5, iceberg-rafted debris (IRD). Vertical profiles of individual fractions and clay mineral content (wt%), water calculated content (Water cont.; wt%), along with clay minerals/clastic minerals, Qz/Pl, and Al/Si ratios. Dating model (solid line) and changes in sedimentation rates (dashed line). The arrows show the reference horizons of the age model and the corresponding dates (see Tables 1 and 2, Supplementary Table 1). cal yr BP calculated by linear interpolation for a surface sample corresponding to AD 2015 (see Tables 1 and 2).

RESULTS

Stratigraphy

Chronostratigraphy and sedimentation rate

Reliable information on sedimentation history over the recent decades was provided via the activity of short-lived radionuclides, such as ^{210}Pb and ^{137}Cs, with half-lives of 22.3 and 30.174 yr, respectively (Koide et al., 1972; Kuptsov, 1986; Sapozhnikov et al., 2006; Supplementary File 1). The subsurface peak of ^{137}Cs activity at 8–10 cm presumably reflects global fallout from nuclear weapon tests in AD 1958 to AD 1963 (Supplementary Fig. 1). However, accumulation of technogenic radionuclides in the fjord sediments occurs with some delay, because the bulk of radionuclides from the atmosphere initially accumulate on the surface of the snow and ice cover and only then enter the fjord (with the meltwater). Therefore, it can be presumed that the sediment layer at 8–10 cm could have accumulated between 1960 and 1970. This is consistent with the results of the AMS ^{14}C–dated sample from 6 to 12 cm (average 9 cm; Tables 1 and 2). The sedimentation rates derived from ^{137}Cs measurements were also found to be in good agreement with sedimentation rates estimated by "excess" ^{210}Pb (Supplementary Fig. 1), both differing from linear sedimentation rates based on the AMS ^{14}C dating by 5–7 yr in the upper 26 cm of the core. This allowed us to accept the dating model shown in Figure 2 and presented in

Supplementary Table 1 as the basis for reconstructing the sedimentation history of the Oga Fjord over the last millennium.

The core sequence can be subdivided into three sections using the down-core variability in sedimentation rates (Fig. 2). The upper section, 0–100 cm, corresponding to the last ca. 415 yr is characterized by the lowest sedimentation rates, close to 0.2–0.25 cm/yr. The middle section, 100–160 cm, accumulated over 70 yr between AD 1600 and AD 1530 under the highest sedimentation rates of 0.86 cm/yr. The lower section, 160–402 cm (AD 1090 to AD 1530), is characterized by moderate average sedimentation, close to 0.55 cm/yr.

Lithostratigraphy

Core AMK-5248 largely consists of reduced medium dark-gray sediments (N4 according to the Munsell Rock Color Chart), with patches of darker, almost black, hydrotroilite spots, except the uppermost 0–2 cm oxidized layer, which is colored a dark greenish-gray to dark-gray (5GY4/1–N3). The upper 12-cm-thick unit is distinguished by high water content of 40–50 wt% (Fig. 2). As the sediments gradually get denser down core, the water content decreases to ~30 wt% at 19–25 cm and remains close to this value in the rest of the core. During onboard visual description, laminated sediments were recorded in the lower part of the core, along with coarse-grained inclusions at 276–319 and

Table 1. The specific activity of short-lived radionuclides in Bq/kg in sediments of core AMK-5248, the standard deviation (Δ), mass of samples, and estimated age of horizons.

Horizons (cm)	^{210}PbΣ	Δ	^{137}Cs	Δ	^{226}Ra	Δ	^{210}Pb excess	Δ	Sample weight (g)	Age (AD)
0–2 (1)	178	±18	3.7	±0.3	13	±1	165	±20	76.61	2015–2000
2–4 (3)	175	±19	4.8	±0.4	16	±1	159	±21	69.86	1995
4–6 (5)	95	±11	3	±0.4	16	±1	79	±15	109.66	1985
6–8 (7)	61	±7	1.3	±0.2	11	±1	50	±9	147.1	1975
8–10 (9)	60	±8	1.9	±0.1	18	±1	42	±10	152.62	1965 (1970[a])
10–12 (11)	59	±7	0.9	±0.1	23	±2	36	±10	168.48	1955
12–14 (13)	60	±8	0.6	±0.2	27	±2	33	±10	103.45	1945
14–16 (15)	36	±5	0.3	±0.1	11	±1	25	±8	149.82	1935
16–18 (17)	26	±6	0.5	±0.2	9	±1	17	±4	102.29	1925
18–20 (19)	19	±3	0.5	±0.1	7	±1	12	±3	120.26	1915
20–22 (21)	18	±3	0.5	±0.1	7	±1	11	±3	135.09	1905
22–24 (23)	10	±5	0.3	±0.1	6	±1	4	±1	144.87	1895
24–26 (25)	16	±2	0.4	±0.1	9	±1	7	±2	128.46	1885

[a]Calendar age calculated by linear interpolation for a sample with modern accelerator mass spectrometry ^{14}C age (see Table 2).

Table 2. Accelerator mass spectrometry ^{14}C dating of carbonate benthic foraminiferal shells (bulk) from core AMK-5248 and the corresponding calendar age calibrated using the Calib Rev v. 8.1.0 (www.calib.org) with the Marine20 calibration curve.

Laboratory number	Horizons (cm)	^{14}C yr BP	Calibrated age (±2σ), (cal yr BP)[a]	Median calendar age (cal yr BP)[a]	Calendar age (AD)
Poz-85993	6–12 (9)	105.7 ± 0.3 pMC	Post-bomb (>1950)	45 ± 0.3	1970
Poz-85994	100–102 (101)	875 ± 30	345–475	415	1600
Poz-85995	160–162 (161)	965 ± 30	425–545	485	1530
Poz-85996	400–402 (401)	1470 ± 30	855–975	925	1090

[a]Calendar age calculated for a surface sample corresponding to AD 2015 (see Table 1).

335–366 cm. Otherwise, the core sequence appeared visually relatively homogeneous.

Based on the grain-size analysis, two granulometric types are distinguished: silt and clayey silt (Fig. 3, Supplementary Table 2). In our analysis, silty sediment is dominated by a coarse silt (0.01–0.063 mm) fraction that constitutes 60–80 wt%. Clayey–silty sediment contains equal amounts (20–40 wt%) of the three finest fractions: coarse silt, 0.01–0.063 mm; fine silt, 0.002–0.01 mm; and clay <0.002 mm. Both granulometric types are characterized by extremely low gravel (0–0.8 wt%) and sand (0–3.8 wt%) content, indicating a predominant supply of fine suspended glacial material (with meltwater) and a relatively limited IRD input.

Statistical analysis revealed more variables than those used to establish granulometric types and included five sand-sized and two silt-sized fractions (Supplementary Table 2). According to a previous study, subdivision of the core sequence based on statistical clustering is more accurate than that based solely on the types (Rusakov et al., 2017, 2018). Factor analysis of grain-size data revealed the two main significant factors that explain the effect of different fractions on the composition (Fig. 4). Factor 1 explains 62.6% of the dispersion and reflects the effect of gravel–sand material >0.063 mm (positive values of the factor;

Fig. 4a). Factor 2 explains 29.5% of the dispersion and represents the competition between the fractions of coarse silt (0.063–0.01 mm; negative factor values) and the total content of fine silt and clay (<0.01 mm; positive factor values).

The graph of factor value (load) distribution in the space of the first two most significant factors (Fig. 4b) and cluster dendrogram (Fig. 4c) display three clusters/granulometric units (GU): GU I, GU IIa, and GU IIb. The low affinity between GU I and GU II (Fig. 4c) is associated with gravel and sand. Notably, the sediments of GU I, with increased IRD input, consist predominantly of fine-grained material.

GU IIa includes sediments having a high coarse silt fraction contribution. As a rule, the increase in coarse silt in the sediments of tidewater fjords is associated with their proximity to the glacial front, where discharge of meltwater and suspended glacial sediment load takes place (proximal glaciomarine sediments; Syvitski, 1989; Ó Cofaigh and Dowdeswell, 2001; Murdmaa et al., 2004; Polyak et al., 2004; Meire et al., 2017).

GU IIb corresponds to sediments with a high content of fine silt and clay fractions <0.01 mm. This material reflects suspension-rich surface glacial–meltwater plumes, also called "glacial milk," and containing a large amount of the suspended glacial matter.
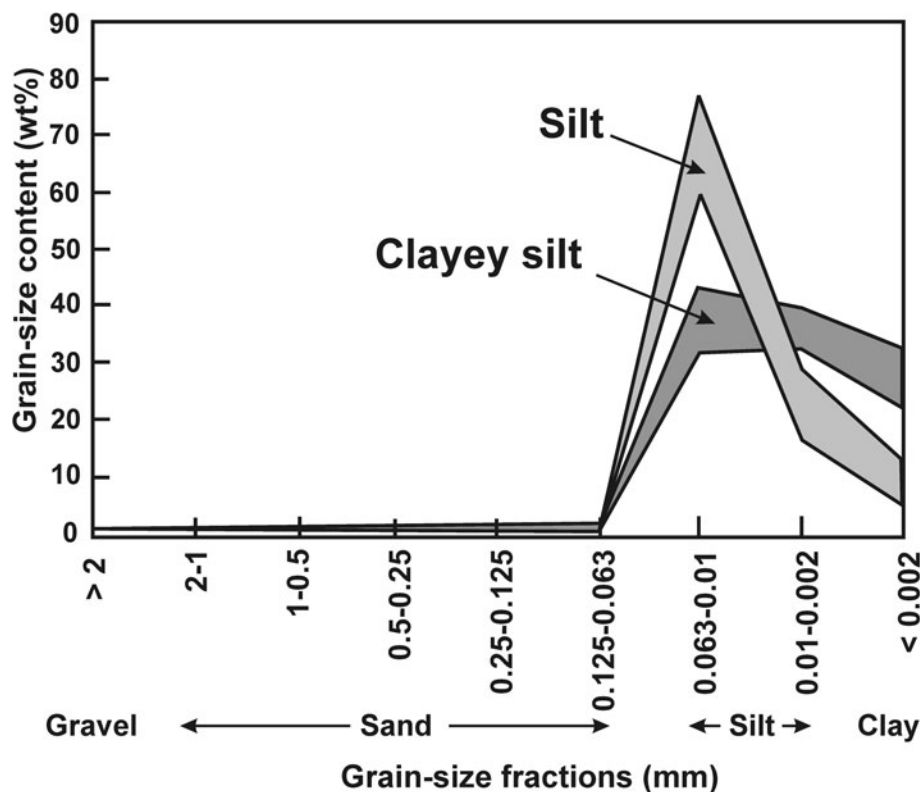
Figure 3. Percentage (wt%) of individual fractions of sediments in core AMK-5248 indicating granulometric types: silt and clayey silt. See also Supplementary Table 2.

Chemostratigraphy

The down-core distribution of chemical elements in core AMK-5248 was found to be rather uniform. The use of trace elements is limited, as most of the variation in their content is close to the statistical error of chemical analysis (Supplementary Table 4), and variations in the content of major elements were only slightly higher: SiO_2 (55.2–56.4 wt%), Al_2O_3 (16.2–17.4 wt %), Fe_2O_3 (7.4–7.9 wt%), MgO (2.71–3.53 wt%), and CaO (1.97–2.88 wt%). For comparison, in the Kara Sea sediments, the major and trace element content varies within 40% (Rusakov et al., 2017, 2018). To derive the relevant information from such a homogeneous geochemical data set, we applied methods of mathematical statistics (Davis, 1990), which allowed us to unravel the "hidden" relationships between chemical elements inaccessible to other geochemical analysis methods. The application of mathematical statistics allows the widest possible range of data on elemental composition of sediments to be used as opposed to, for example, geochemical modules, for which only a finite set of chemical elements is used.

Factor analysis revealed the two main significant factors that together explain 63.6% of the variance in the chemical composition of sediments (Fig. 5a). The remaining factors had low significance. Factor 1 explains 34.4% of the variance and represents competition between Si, Ti, Fe, Mg, and K (positive factor values) and Al, Ca, P, and Mn (negative factor values). Factor 2 explains 29.2% of the variance and reflects the competition between Si, Ca, Mg, and P (positive factor values) and Al and K (negative factor values).

Chemical elements that show the highest dispersion are plotted in the factor space of the first two factors in Fig. 5b. Here, the factor space is divided into four quadrants, each reflecting a certain combination of factor signs, similar to the factor space shown in Fig. 4b for grain-size composition. However, in contrast to the grain-size factor values, positions of individual chemical elements in the factor space do not form independent clusters. For this reason, further classification of chemical elements is based on their position in the corresponding factor space quadrant. The established chemical quadrants are referred to as chemical units (CU; Supplementary File 2).

Mineralogy

The mineral composition of 27 sediment samples (Supplementary Table 3) demonstrated equal representation of clastic and clay minerals. Quartz and plagioclase predominated among clastic (bulk non-clay) minerals, accounting for ∼43 wt% in total. The average proportion of quartz was approximately two times higher than that of plagioclase (Fig. 2, Supplementary Table 3). The remaining clastic minerals accounted for 5–6 wt% (ankerite, 2.3 wt%; calcite, 2.2 wt%; potassium feldspar, <0.9 wt%; and dolomite, <0.9 wt%). The presence of these carbonate minerals indicates Paleozoic terrigenous-carbonate beds as a potential source of sedimentary material (Lopatin, 1999). Notably, biogenic calcite was significantly less abundant than clastic calcite (<<1 wt%).

The total content of clay minerals (illite, chlorite, and kaolinite) exceeded 50 wt%, allowing us to refer the studied sediments as siliciclastic clay, according to the accepted lithologic classification (Frolov, 1993; Boggs, 2009; Prothero and Schwab, 2013). Among them, illite is the main clay mineral, accounting for an average of 32.8 wt% of the total mass. Notably, the sum clay mineral content was higher than the clay fraction (Fig. 2, Supplementary Tables 2
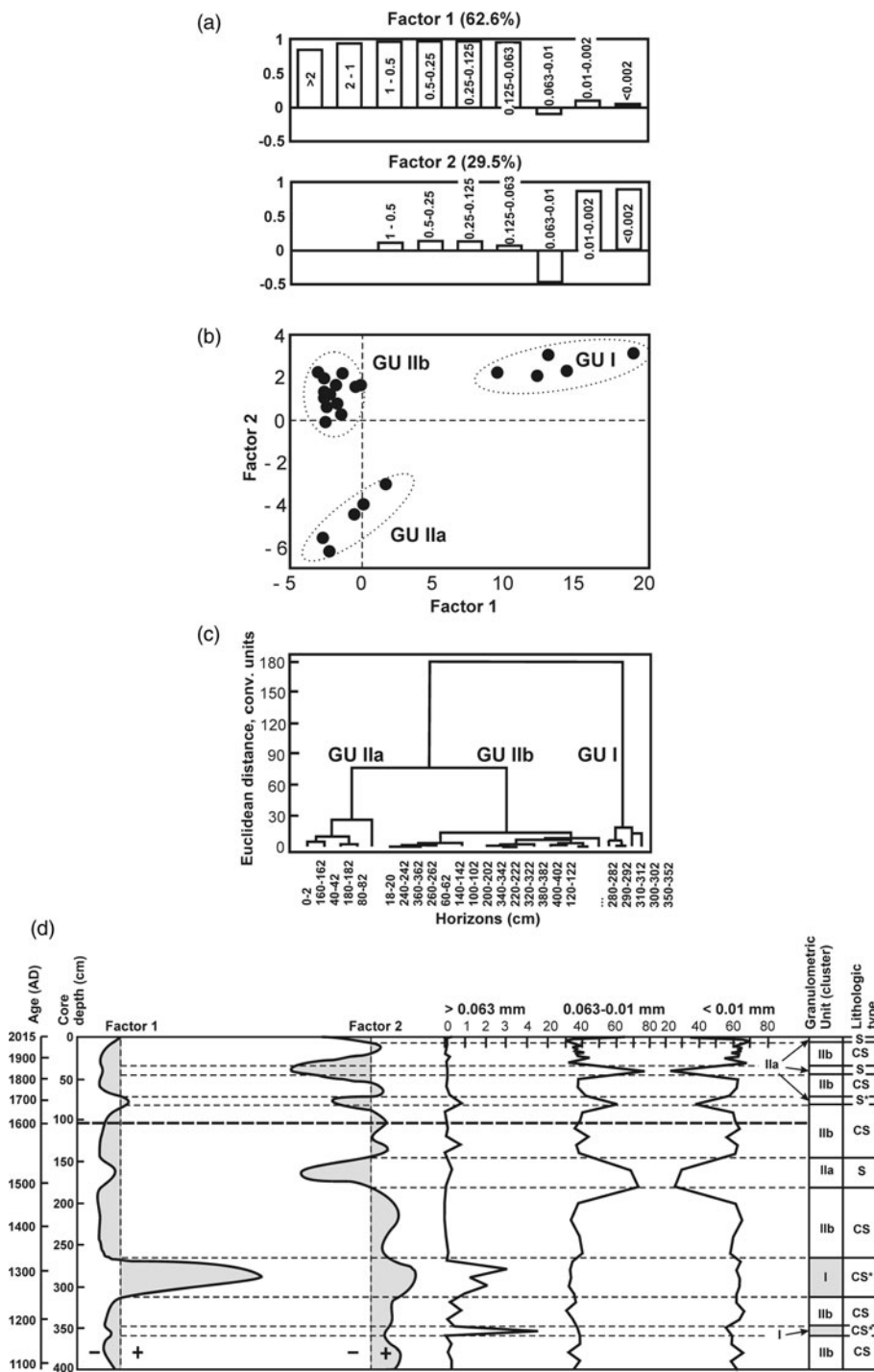
Figure 4. Results of factorial and cluster analyzes of the grain-size composition of sediments of core AMK-5248: (a) most significant factors and their load in %; (b) distribution of values in the factor space of the first two factors; (c) dendrogram of hierarchical connections between individual horizons: cluster/granulometric unit I (clayey silt with inclusion of gravel–sand material), cluster/granulometric unit IIa (silt), and cluster/granulometric unit IIb (clayey silt; Supplementary Table 2); and (d) vertical distribution of the first two factors along the core and granulometric type division: S (silt), CS (clayey silt), S* (silt with iceberg-rafted debris [IRD] inclusions), and CS* (clayey silt with IRD inclusions).

and 3). This indicates that some of the clay minerals grains were larger than 0.002 mm.

On triangular diagrams in the coordinates "quartz–plagioclase–sum of clay minerals" (Fig. 6a), as well as in coordinates "illite–chlorite–kaolinite" (Fig. 6b), all studied samples form a local area. This indicates both a homogeneous source of sedimentary material and a weak reaction of the mineral composition of these terrigenous siliciclastic clayey sediments to changes in sedimentation conditions over the last millennium. Minor down-core changes in mineral composition likely result from hydraulic differentiation of sedimentary material within the fjord in relation

to glacial front shifts, sea-ice conditions, and water circulation (Supplementary File 3).

Rare earth elements and yttrium
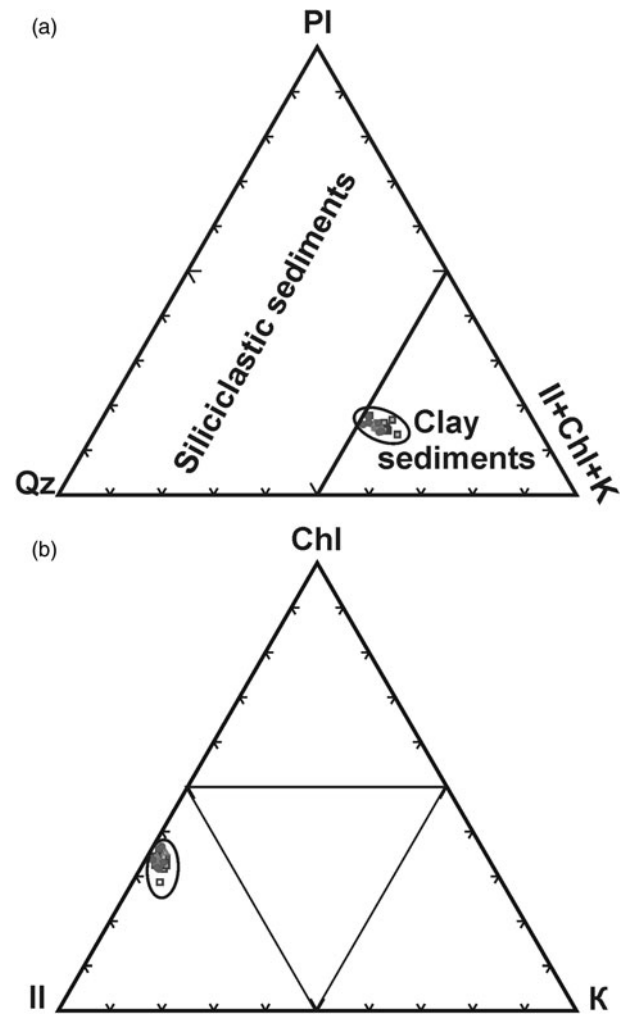
The down-core records of REY content were extremely uniform. The ratios of light REE to heavy ones, expressed as La/Yb and LREE/HREE, varied within a very narrow range, amounting to 10.5 ± 1.0 and 1.1 ± 0.1, respectively (Supplementary Table 5). The correlation between these ratios was high, as was evident from the accuracy of the approximation ($R^2 = 0.78$). The ratios
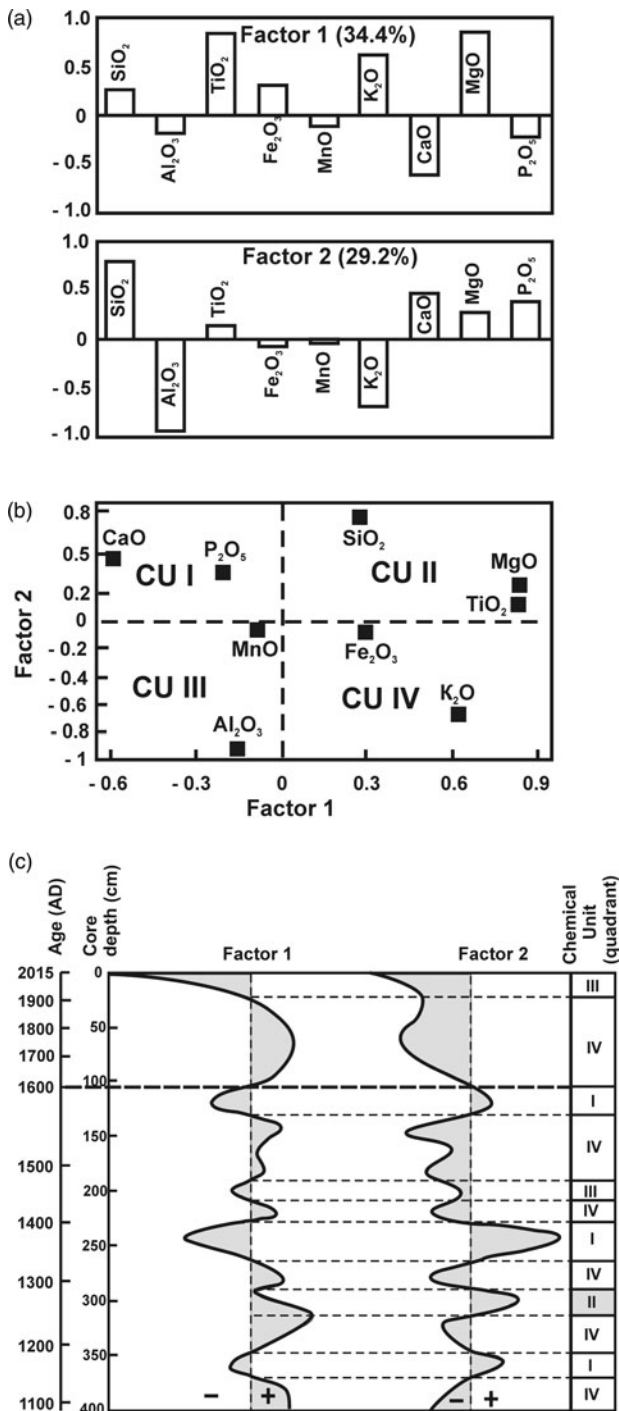
Figure 5. Results of factor analysis of chemical composition of sediment of core AMK-5248: (a) the most significant factors and their load in %; (b) distribution of values in the factor space of the first two factors; and (c) vertical distribution of the first two factors along the core and chemostratigraphic division. See also Supplementary Table 4.


Figure 6. Triangular diagrams of mineral composition of sediments of core AMK-5428: (a) in coordinates: quartz (Qz)–plagioclase (Pl)–the sum of clay minerals; (b) in coordinates: illite (Il)–chlorite (Chl)–kaolinite (K). See also Supplementary Table 3.

indicate an intermediate position of the studied sediments between sandstones having high quartz content and shales. They also differed from the reference composition of shales (North American shale composite [NASC]; Gromet et al., 1984) in their relatively low REY content due to the influence of clastic minerals. This conclusion is confirmed by the low total content of REE (ΣREE = 130 ± 5 ppm), which also corresponds to an intermediate position between sandstones and shales (Taylor and

McLennan, 1985). The studied sediments differed from NASC because of high europium anomaly (Eu/Eu* = 1.06 ± 0.2), which indicates a considerable contribution of plagioclase (Taylor and McLennan, 1985). Thus, the composition of REY in core AMK-5248 largely reflects the mineral composition of sediments characterized by a mixture of clay minerals and clastic minerals in proportions close to 50/50, together with a high representation of quartz (28.8 wt%) and plagioclase (14.6 wt%) among the clastic group (Supplementary Table 3).

The REY composition curves, normalized to the average composition of NASC, roughly correspond to the composition of Holocene sediments of the Kara Sea (Fig. 7, Supplementary Table 5). Meanwhile, their distribution pattern and total REY content are in good agreement with the sediments of the southern part of the Novaya Zemlya Trough (Rusakov et al., 2018), which is a natural trap for sedimentary material carried by the eastern glaciers of Novaya Zemlya.

Similar to the mineral and chemical compositions, the uniform distribution of REY in core AMK-5248 indicates a single source of sedimentary material, that is, a Paleozoic (Ordovician–Permian) bedrock represented by terrigenous–marine sedimentary complex with thin layers of carbonates (Lopatin, 1999).
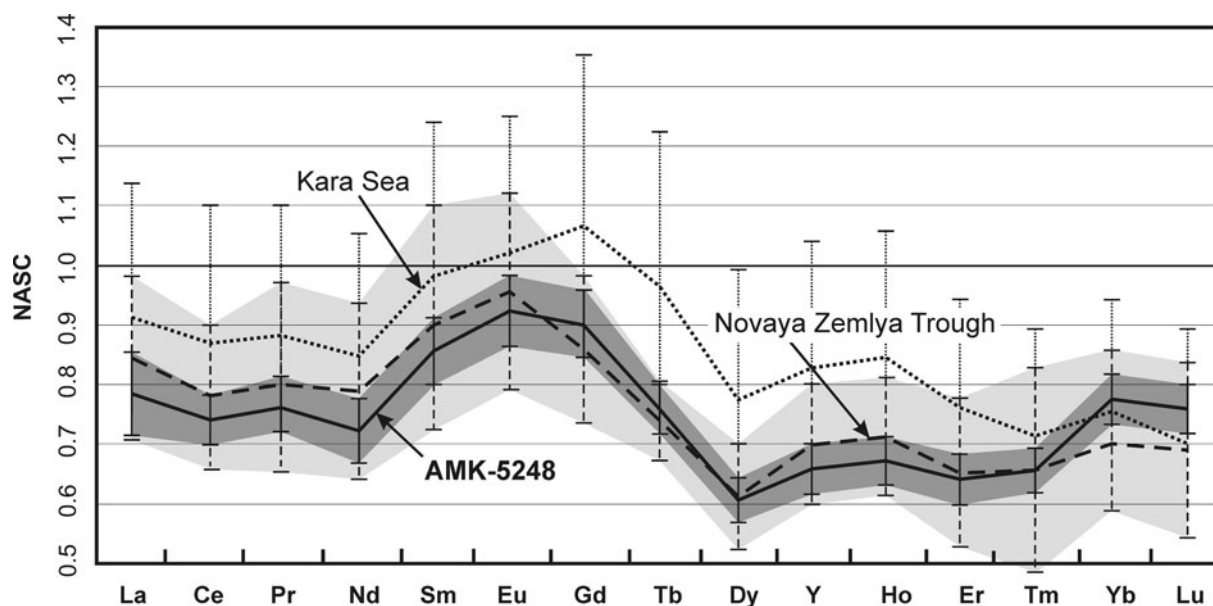
Figure 7. Range of composition values for rare earth elements and yttrium (REY) content in sediments of core AMK-5248 (highlighted darker; data from this work), as well as the clayey and clayey silty surface (0–2 cm) bottom sediments of Kara Sea and Novaya Zemlya Trough (highlighted lighter; Rusakov et al., 2018), normalized to the composition of the North American shale composite (NASC; Gromet et al., 1984). The curve of average composition of core AMK-5248 is shown as a solid line. The curves of average composition of Kara Sea and Novaya Zemlya Trough are shown as dotted lines. See also Supplementary Table 5.

DISCUSSION

Major glaciological factors affecting proximal glaciomarine sediment

From the point of view of lithologic facies analysis, the studied sediment core AMK-5248 belongs to proximal glaciomarine sediments accumulated in the immediate vicinity of the glacial front (Syvitski, 1989; Ó Cofaigh and Dowdeswell, 2001; Murdmaa et al., 2004; Polyak et al., 2004; Meire et al., 2017). In general, the use of the proximal glaciomarine sediments for paleoreconstructions has significant limitations, due to the relatively homogeneous composition of the sediments. As shown earlier, noticeable changes along the core are observed only for the grain-size and chemical composition of sediment (Figs. 4d and 5c, Supplementary Tables 2 and 4), while for the mineral and REY composition of sediment (Figs. 3 and 7, Supplementary Tables 3 and 5), they are almost invisible. Based on this, the major factor affecting the change in the sedimentation in the fjord is sedimentation rate, which indicates both a distance to the glacial front and glacial dynamics. In turn, these factors are determined, first of all, by the external glaciological factors (Meier and Post, 1969; Clarke, 1987; Eisen et al., 2001; Copland et al., 2003; Nesje and Dahl, 2003; Matthews and Briffa, 2005), which are highly dependent on changes in temperature and the amount of atmospheric precipitation. Ice temperature largely controls the speed of glacial ice movement, and the precipitation affects glacial mass-balance conditions. The cumulative effect of these two main factors will ultimately determine the intensity and composition of the sediment discharged into the fjord. Based on their combination, at least four scenarios for the development of depositional/environmental events are assumed. (1) Cooling combined with a decrease in atmospheric precipitation will contribute to a decrease in the dynamics of glacial ice movement, stabilization of the glacial front, and a decrease in the intensity of iceberg calving. (2) Cooling combined with an increase in atmospheric precipitation will contribute to an increase in the volume of an ice cap and a glacial frontal advance. Both scenarios are expressed in a decrease in sedimentation rates and accumulation of the finest sediment in the fjord. (3) Warming combined with a decrease in atmospheric precipitation will contribute to an active glacial frontal retreat, accompanied by an increase in meltwater runoff. Accordingly, (4) warming combined with an increase in atmospheric precipitation will initiate an active iceberg calving and an intense meltwater discharge. The last scenario assumes the highest sedimentation rates, accompanied by the accumulation of sediment of wide grain-size composition.

The internal glaciological factor influencing the sedimentation in the fjord is the rapid and short-term movement of the glacial ice ("surge"; Dowdeswell and Williams, 1997; Eisen et al., 2001; Evans and Rea, 2003; Grant et al., 2009). Despite the fact that the Goluboi tidewater glacier is not classified as a surge-type (Kotlyakov 1978; Grant et al., 2009), periodic sandy and gravel–sand interlayers in core AMK-5248 (Fig. 2) may indicate short-term periods of rapid glacial movement accompanied by active iceberg calving.

Paleoreconstruction

Time period AD 1090 to AD 1600

The stratigraphical division of the core AMK-5248 based on the study of its grain-size and chemical composition (granulometric and chemical units; Figs. 4d and 5c) made it possible to identify the main stages of sedimentation history in the Oga Fjord. The earliest stage, according to the accepted age model (Fig. 2, Supplementary Table 1), dates back to the time period before AD 1600. The sediments of this time can be conditionally divided into two parts, accumulated before and after AD 1300. Stratified sediments accumulated before 1300 are characterized by a higher content of coarse fractions and the highest amount of IRD (Figs. 2 and 8). This period coincides in time with the warm Medieval
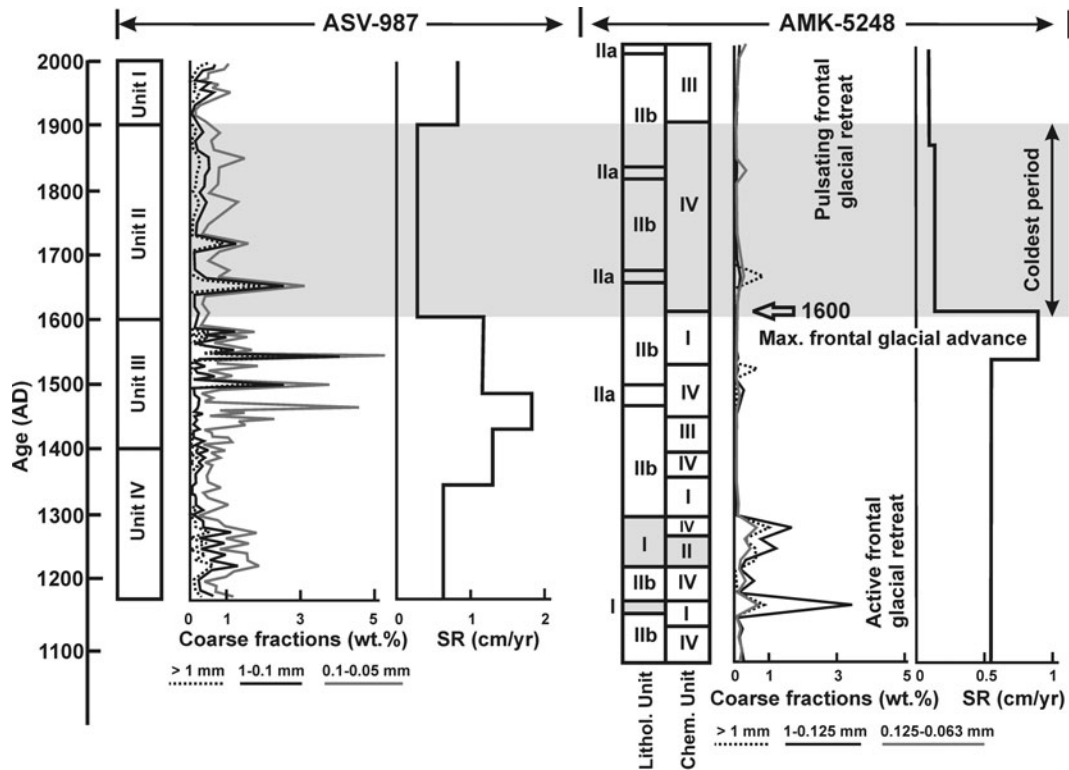
Figure 8. Subdivision of core AMK-5248, based on lithostratigraphy and chemostratigraphy (data from this work) and core ASV-987 (Murdmaa et al., 2004; Polyak et al., 2004). SR, sedimentation rate.

Climate Anomaly (MCA). It should be noted that the stratified sediments are not traced higher along the core. This suggests this is the warmest period in the fjord's sedimentation history before AD 1300.

Sediments of GU IIb (clayey silt) predominated in core AMK-5248 (Fig. 4d, Supplementary Table 2). They alternated with sediments of GU IIa (silt) in the upper part of the core (0–180 cm; after AD 1495), whereas they alternated with sediments of GU I (IRD-enriched clayey silt) in its basal part (280–402 cm; before AD 1315). The time period before AD 1300 was characterized by high supply of coarse fractions (sand and gravel-sand; Fig. 2). CU II that coincides with the sediments of the IRD peak (300–312 cm, AD 1255–1275) points to a warming peak in the second half of the thirteenth century and the important role of elements such as Si, Ti, and Mg (Fig. 5b), indicating high content of quartz and other clastic minerals (Supplementary Files 2 and 3). In general, the warmest epoch before AD 1300 was characterized by a frontal glacial retreat accompanied by active meltwater discharge and iceberg calving in the Oga Fjord (Fig. 8).

The alternation of GU IIa and GU IIb in the upper part of the core points to an unstable hydrodynamic regime in the fjord after AD 1300, most likely associated with glacial dynamic instability. It is important to note that the outlined transition to a cooling, first of all, was reflected in the change in the chemical composition of sediment. Around AD 1275, CU II was replaced by CU IV (Fig. 5c). The change in grain-size composition occurs with a slight delay (Fig. 8). This indicates that changes in the chemical composition of the studied sediments are more sensitive to changes in sedimentation conditions.

Sediments accumulated after AD 1300 are characterized by a finer grain-size composition (Fig. 4d, Supplementary Table 2) and coincide in time with the gradual transition from the warm MCA to the cooling of the early Little Ice Age (LIA). During this period, the granulometric type of the sediment remains practically unchanged (GU IIb), except for the 160–182 cm horizon (AD 1495 to AD 1535), corresponding to the coarser GU IIa sediment (Fig. 4d). As mentioned earlier, the GU IIa sediment can be associated with a short-term surge event (Grant et al., 2009 and references therein). At the same time, the chemical composition of sediments varied widely (CU I, III, and IV; Fig. 5c, Supplementary Table 4), indicating short-term changes in sedimentation conditions. From the fine-grained sediment composition (GU IIb), in combination with the near absence of IRD, it is possible to assume severe sea-ice conditions during the entire fourteenth century. The relatively high Mn content in CU III (Fig. 5b) indicates a good aeration of the water column (Supplementary File 2), likely due to active vertical water circulation caused by the formation of brines when the seawater freezes.

Sedimentation rates before AD 1530 were around 0.55 cm/yr, but then sharply increased up to 0.86 cm/yr (Figs. 2 and 8), indicating the highest meltwater runoff carrying large amounts of the insoluble glacial matter into the fjord and/or the frontal glacial advance. A drastic increase in the sedimentation rate was also reflected in the change in the chemical composition of sediment (Figs. 5c and 8). The highest sedimentation rates are characterized by the accumulation of CU I sediments, reflecting the highest role of Ca and P (Fig. 5b, Supplementary File 2). The main source of Ca is clastic minerals such as Ca-rich plagioclase, ankerite, calcite, and dolomite (Supplementary Table 3), while the source of P is

possibly insoluble organic matter discharged into the fjord by glacier.

Similar warm environmental conditions for the MCA (denoted as AD 1170 to AD 1400) were reconstructed in the Russkaya Gavan' Fjord on the west coast of North Island facing the Barents Sea (Murdmaa et al., 2004; Polyak et al., 2004). Sedimentation rates on the west coast were higher (1.0 cm/yr; Fig. 8), most likely due to the stronger dynamics of the western glaciers, which are influenced by Atlantic cyclones carrying a large amount of moisture. According to Glazovsky (2003), the west coast of the archipelago receives 600 mm/yr more atmospheric precipitation than the east coast. There is also a difference in the snow accumulation pattern between glaciers located on the west and east coasts of North Island (Chizhov et al., 1968; Zeeberg and Forman, 2001; Polyak et al., 2004). At AD 1380, the sedimentation rate in the Russkaya Gavan' Fjord increased twofold to 1.3 cm/yr, and later, between AD 1434 and AD 1488, reached a maximum of 1.8 cm/yr (Fig. 8). Together with distinct coarse lamination, increase in silt to fine sand fraction content, and the presence of clay pellets, the sharp rise in sedimentation rates indicates a rapid frontal glacial advance and/or the highest meltwater runoff carrying large amounts of the insoluble glacial matter into the fjord during the fourteenth and fifteenth centuries.

The oxygen isotopes and Na content in the ice-core records of Svalbard, Franz Josef Land, and Severnaya Zemlya indicate three main stages of climate change in the Arctic during the eleventh to sixteenth centuries (Opel et al., 2013). During the eleventh and twelfth centuries, in general, a warm climate prevailed. After AD 1300, an unstable climate with changeable atmospheric circulation is noted. Since the middle of the fifteenth century, the amount of atmospheric precipitation has increased, probably influencing the dynamics of the glacial ice movement and the frontal glacial advance on Novaya Zemlya. This is the main reason behind the dramatic increase in sedimentation rates in the fjords (Fig. 8).

Coldest time period AD 1600 to AD 1920

Around AD 1600 in the Oga Fjord, sedimentation rate decreases fourfold from 0.86 to 0.25 cm/yr (Figs. 2 and 8). The only explanation for such a drastic decrease in the supply of sedimentary material to the fjord is a significant slowdown or "stop" of the glacial movement caused by a sharp cooling in combination with a decrease in the amount of atmospheric precipitation. It should be noted that only a change in the chemical composition of the sediments is noted at this time. CU I is replaced by CU IV, reflecting the change in the leading role of Ca and P to Fe and K (Fig. 5b). Presumably, this reflects a slight increase in the proportion of K-rich minerals in sediments, such as potassium feldspar and illite, as well as Fe oxyhydroxides and hydrotroilite (Supplementary File 2). A change in the grain-size composition of sediment (GU IIa, silt with gravel-sandy material inclusions; Supplementary Table 2) is noted only at the horizon of 80–82 cm (AD 1685), that is, about 85 yr after the sharp decline in the sedimentation rate. This sediment coarsening could have been caused by a short-term frontal glacial advance into the fjord in combination with iceberg calving, which both followed its slowdown/stop glacial dynamics. The late LIA, after 1600 AD, stands out as the coldest period in the Oga Fjord, with the lowest glacial dynamics, almost no meltwater impact, and severe sea-ice conditions, as indicated by low sedimentation rates, no IRD, and predominantly fine-grained sediment (Fig. 8). Further, until the end of the nineteenth century, no significant changes were observe in either the grain-size or chemical composition of sediments, which indicates the stabilization of the coldest and driest climate during the late LIA.

A synchronous and drastic decrease in sedimentation rates is also noted in the Russkaya Gavan' Fjord. After AD 1600, the sedimentation rates in core ASV-987 dropped threefold and remained low until the beginning of the twentieth century (Murdmaa et al., 2004; Polyak et al., 2004; Fig. 8). A possible reason for such significant climatic changes, both on the east and west coasts of Novaya Zemlya, was the explosive eruption of the Huaynaputina volcano, AD 1600, in southern Peru (Thouret et al., 1999). According to the chronicles, the eruption lasted from February 19 to March 6 and became the largest explosive eruption in historical times in the Andes. It is believed that this eruption could have caused great climatic changes during the LIA (Verosub and Lippman, 2008; Witze, 2008). According to Witze (2008), the eruption may have had a far wider effect, injecting sulfur particles high into the atmosphere and disrupting the climate worldwide. This is corroborated by tree-ring records showing that it was the coldest year in six centuries in the Northern Hemisphere (Verosub and Lippman, 2008 and references therein). It could also have caused the Great Famine of AD 1601 to AD 1603 (Boguslavskiy, 2004), which led to the change of the ruling dynasties in Russia. In the Russian annals, it is written (Karamzin, 1829; page 704): "In the spring of 1601, the sky was clouded with thick darkness and the rains poured incessantly for ten weeks … On August 15, a severe frost damaged the unripe bread (*rye*) and all the fruits." Despite the fact that direct evidence of a connection between these events has not yet been found, the difference between them is only a year. The drastic decrease in sedimentation rates in the fjords of Novaya Zemlya that we discovered, which are synchronous with the described events of the eruption and famine, may be an additional fact confirming the influence of the eruption in Peru on the global climate.

The frontal retreat of the Goluboi tidewater glacier after its maximum progradation in the sixteenth century occurred in pulses, with periods of stabilization and short-term frontal glacial readvances (glacial surges; Grant et al., 2009), when the sediment composition became coarser (GU IIa; Figs. 4d and 8). Similar cold climatic conditions were reconstructed in the Russkaya Gavan' Fjord during AD 1600 to AD 1900 (Murdmaa et al., 2004; Polyak et al., 2004). Cold regional conditions were also clearly recorded in the oxygen isotopic composition of the ice core of Severnaya Zemlya, with a maximum in AD 1760 to AD 1800 followed by a gradual warming until the early twentieth century (Opel et al., 2013). According to the Na content of this ice core, the most severe sea-ice conditions were recorded in the earliest nineteenth century. A similar pattern in the oxygen isotope composition changes characterizes ice-core records in Svalbard and Franz Josef Land (Opel et al., 2013). Analysis of numerous proxy data sets revealed a general circum-Arctic summer cooling during the century-long period of AD 1766 to AD 1865, with the coldest decade being AD 1811 to AD 1820 (Werner et al., 2018). Cold environmental conditions and the relatively stable position of the glaciers on Novaya Zemlya during the eighteenth and nineteenth centuries were coeval with frontal glacial advances in western Norway and Svalbard (Nesje and Dahl, 2003; Mangerud and Landvik, 2007; Nesje et al., 2008; Majewski et al., 2009). Mean surface atmospheric circulation in the Kara Sea region facilitates the transport of continental air masses with a low amount of moisture (Moore, 2013; Dubinina et al., 2020). As a result, the

Novaya Zemlya glaciers experience a precipitation deficit compared with Svalbard, which is more strongly influenced by humid Atlantic cyclones. However, this also might have been a result of the shift in the tracks of winter cyclones during the late LIA (Zeeberg and Forman, 2001; Nesje and Dahl, 2003; Matthews and Briffa, 2005; Nesje et al., 2008; Luoto and Helama, 2010; D'Andrea et al., 2012).

Time period AD 1920 to AD 2015
The warming in the early twentieth century is characterized only by a change in the chemical composition in the AMK-5248 core (Figs. 5c and 8). The CU III sediment reflects the leading role of Mn and Al (Supplementary File 2), indicating an increase in aeration of the water column and an increase in role of clay minerals in sediment, respectively. In turn, the aeration reflects the conditions of the fjord's prolonged seasonal opening from sea ice, and the accumulation of clay minerals could be explained by the glacial front's distant position from sampling site. Perhaps position of the glacier in retreat was partially retained after the previous cold eighteenth and nineteenth centuries and later enhanced by active thinning occurring during the twentieth century. Sediment coarsening was noted only for the upper 2 cm of the core (GU IIa; Supplementary Table 2), dated AD 2000 to AD 2015 (Table 1). It is possible that the change in the grain-size composition of sediment is associated with an increase in the amount of atmospheric precipitation and a steady rise in surface air temperatures over the past decades.

In the Russkaya Gavan' Fjord, warming and active glacial thinning are reconstructed on the basis of an increase in sedimentation rates, growing bioproductivity, and two pronounced stable isotope minima during the early twentieth century and recently (Murdmaa et al., 2004; Polyak et al., 2004). Although the climatically induced environmental changes on the east and west coasts of Novaya Zemlya are almost synchronous, sedimentation rates are higher in the west. This is likely the result of the climate on the Kara Sea coast being the colder and drier than on the maritime Barents Sea coast. The last 100 yr were generally characterized by rapid widespread warming in the Arctic and subarctic regions (Kaufman et al., 2009; PAGES 2k Consortium, 2013). In the ice-core records of Severnaya Zemlya, warming is indicated by the absolute maximum surface air temperatures, manifested by positive shifts in oxygen isotope composition and highest Na content, especially in the early twentieth century (Opel et al., 2013). Matusevich and Sokolov (1927), in their monograph *Novaya Zemlya*, describe the results of the geographic exploration of the east coast of Novaya Zemlya. Although they do not provide the data on glacial front positions and sea-ice regime, they state that, until the 1920s, the exploration of the Kara Sea was only possible with an icebreaker. Nowadays, summer expeditions to the Kara Sea are conducted on ships of a non- icebreaker class. This clearly indicates rapid climate change and summer sea-ice loss.

CONCLUSIONS

Based on the proximal glaciomarine sediment records in the sedimentation history of the Oga Fjord, at least four depositional/environmental periods have been distinguished during the last millennium. The earliest period, before AD 1300, was characterized by the warmest epoch of Novaya Zemlya, accompanied by active frontal glacial retreat, active meltwater discharge, and iceberg calving.

This was followed by a period of paleoenvironmental instability, with a changeable climate between AD 1300 and AD 1600, and it coincides in time with the gradual transition from the warm MCA to the cooling of the early LIA. At the end of this period, AD 1530 to AD 1600, a sharp increase in sedimentation rates is noted, due to an increase in atmospheric precipitation, the intensified dynamics of the glacial ice movement, and the frontal glacial advance on Novaya Zemlya.

The beginning of the seventeenth century is marked by a drastic decrease in sedimentation rates in the fjords, both on the east and west coasts of Novaya Zemlya. This event coincides in time with the largest explosive eruption in historical times of the Huaynaputina volcano in the Andes and the Great Famine (AD 1601 to AD 1603) in Russia. The late LIA, after 1600 AD, stands out as the coldest period in the Oga Fjord, with the lowest glacial dynamics, almost no meltwater impact, and severe sea-ice conditions, as indicated by low sedimentation rates, no IRD, and predominantly fine-grained sediment. At the same time, the coldest period was characterized, in general, by frontal glacial retreat occurring in pulses, with periods of stabilization and short-term frontal glacial readvances. The main reason for this retreat was apparently the systemic deficit of atmospheric precipitation due to a change of atmospheric circulation pattern and a shift in the tracks of winter cyclones.

The last 100 yr were characterized by warming and active glacial thinning. In the Oga Fjord, warming was recorded as sediment coarsening, especially in the first decade of the twenty-first century, possibly due to an increase in the amount of atmospheric precipitation and a steady rise in surface air temperatures.

REFERENCES

Andreeva, I.A., Lapina, N.N., 1998. *Methodica granulometricheskogo analiza donnikh osadkov Mirovogo okeana i geologicheskaya interpretatsiya resultatov laboratornogo izucheniya veschestvennogo sostava* [Method of grain-size analysis of bottom sediments of the World Ocean and geological interpretation of the results of laboratory study]. VNIIOkeangeologia, St. Petersburg.

Batchelor, C.L., Margold, M., Krapp, M., Murton, D.K., Dalton, A.S., Gibbard, P.L., Stokes, C.R., Murton, J.B., Manica A., 2019. The configuration of Northern Hemisphere ice sheets through the Quaternary. *Nature Communications* **10**:3713.

Boggs, S., Jr., 2009. *Petrology of Sedimentary Rocks*. 2nd ed. Cambridge University Press, New York.

Boguslavskiy, V.V., 2004. Golod 1601–1603 godov [Famine 1601–1603]. In: *Slavianskaya enziklopedia XVII vek* [Slavic encyclopedia of the 17th century]. Olma Press, Moscow.

Carlson, A.E., Clark, P.U., 2012. Ice sheet sources of sea level rise and freshwater discharge during the last deglaciation. *Reviews of Geophysics* **50**, RG4007.

Carr, J.R., Stokes, C., Vieli, A., 2014. Recent retreat of major outlet glaciers on Novaya Zemlya, Russian Arctic, influenced by fjord geometry and sea-ice conditions. *Journal of Glaciology* **219**, 155–170.

Chizhov, O.P., Koryakin, V.S., Davidovich, N.V., Kanevskii, Z.M., Zinger, E.M., Bazheva, V.Ya., Bazhev, A.B., Khmelevskoi, I.F., 1968. *Oledenenie Novoi Zemli* [Glaciation of the Novaya Zemlya]. Nauka, Moscow.

Clarke, G.K.C., 1987. Fast glacier flow: ice streams, surging and tidewater glaciers. *Journal of Geophysical Research Atmospheres* **92**(B9), 8835–8841.

Clark, P.U., Dyke, A.S., Shakun, J.D., Carlson, A.E., Clark, J., Wohlfarth, B., Mitrovica, J.X., Hostetler, S.W., McCabe A.M., 2009. The last glacial maximum. *Science* **325**, 710–714.

Copland, L., Sharp, M.J., Dowdeswell, J.A., 2003. The distribution and flow characteristics of surge-type glaciers in the Canadian high Arctic. *Annals of Glaciology* **36**, 73–81.

D'Andrea, W.J., Vaillencourt, D.A., Balascio, N.L., Werner, A., Roof, S.R., Retelle, M., Bradley, R.S., 2012. Mild Little Ice Age and unprecedented recent warmth in an 1800 year lake sediment record from Svalbard. *Geology* **40**, 1007–1010.

Davis, J.C., 1990. *Statisticheskii analiz v geologii* [Statistical analysis in geology]. Nedra, Moscow.

Divine, D., Isakson, E., Martma, T., Mejer, H.A.J., Moore, J., Pohjola, V., van de Wal, R.S.W., Godtliebsen, F., 2011. Thousand years of winter surface air temperature variations in Svalbard and northern Norway reconstructed from ice core data. *Polar Research* **30**, 1–12.

Doebelin, N., Kleeberg, R., 2015. Profex: a graphical user interface for the Rietveld refinement program BGMN. *Journal of Applied Crystallography* **48**, 1573–1580.

Dowdeswell J.A., Williams, M., 1997. Surge-type glaciers in the Russian High Arctic identified from. digital satellite imagery. *Journal of Glaciology* **43**, 489–494.

Dubinina, E.O., Chizhova, Ju.N., Kossova, S.A., Avdeenko, A.S., Miroshnikov, A.Yu., 2020. Formation of isotope parameters (δD, δ^{18}O, and d) of glaciers and water runoff from Severny Island of the Novaya Zemlya archipelago. *Oceanology* **60**, 174–188.

Eisen, O., Harrison, W.D., Raymond, C.F., 2001. The surges of Variegated Glacier, Alaska, U.S.A., and their connection to climate and mass balance. *Journal of Glaciology* **47**, 351–358.

Evans, D.J.A., Rea, B.R., 2003. Surging glacier landsystem. In: Evans, D.J.A., (Ed.), *Glacial Landsystems*. Edward Arnold, London, pp. 259–288.

Fairbanks, R.G., 1989. A 17,000-year glacio eustatic sea level records: influence of glacial melting rates on the Younger Dryas event and deep-ocean circulation. *Nature* **342**, 637–642.

Frolov, V.T., 1993. *Litologiya* [Lithology]. Book 2. MGU Press, Moscow.

Gataullin, V., Mangerud, J., Svendsen, J.I., 2001. The extent of the Late Weichselian ice sheet in the southeastern Barents Sea. *Global and Planetary Change* **31**, 453–474.

Gataullin, V.N., Polyak, L.V., Epstein, O.G., Romanyuk, B.F., 1993. Glacigenic deposits of the Central Deep: a key to the Late Quaternary evolution of the eastern Barents Sea. *Boreas* **22**, 47–58.

Glazovsky, A.F., 2003. Glacier changes in the Russian Arctic. In: Casey, A. (Ed.), *Workshop on Assessing Global Glacier Recession*. Glaciological Data Report GD-32. World Data Center for Glaciology, Boulder, CO, pp. 78–82.

Gorshkov, S.G. (Ed.), 1980. *Atlas of the Oceans. Arctic Ocean*. USSR Ministry of Defense, Voenno-Morskoy Flot Press, Moscow.

Grant, K.L., Stokes, C.R., Evans, I.S., 2009. Identification and characteristics of surge-type glaciers on Novaya Zemlya, Russian Arctic. *Journal of Glaciology* **55**, 960–972.

Gromet, L.P., Dymek, R.F., Haskin, L.A., Korotev, R.L., 1984. The "North American shale composition": its complication, major and trace element characteristics. *Geochimica et Cosmochimica Acta* **48**, 2469–2482.

Howe, J.A., Husum, K., Inall, M.E., Coogan, J., Luckman, A., Arosio, R., Abernethy, C., Verchili D., 2019. Autonomous underwater vehicle (AUV) observations of recent tidewater glacier retreat, western Svalbard. *Marine Geology* **417**, 106009.

Hughes, A.L.C., Gyllenkreutz, R., Lohne, Ø.S. Mangerud, J., Svendsen, J.I., 2015. The last Eurasian ice sheets—a chronological database and time-slice reconstruction, DATED-1. *Boreas* **45**, 1–45.

Isaksson, E., Divine, D., Kohler, J., Martma, T., Pohjola, V., Motoyama, H., Watanabe, O., 2005. Climate oscillations as recorded in Svalbard ice core delta O-18 records between AD 1200 and 1997. *Geografiska Annaler, Series A: Physical Geography* **87**, 203–214.

Jernas, P., Klitgaard-Kristensen, D., Husum, K., Wilson, L., Koç, N., 2013. Paleoenvironmental changes of the last two millennia on the western and northern Svalbard shelf. *Boreas* **42**, 236–255.

Karamzin, N.M., 1829. *Istoriya gosudarstva Rossiiskogo. Tom XI. Chast' II* [History of the Russian state. Vol. XI. Part II]. N. Grecha, St. Petersburg.

Kaufman, D.S., Schneider, D.P., McKay, N.P., Ammann, C.M., Bradley, R.S., Briffa, K.R., Miller, G.H., et al., 2009. Recent warming reverses long term Arctic cooling. *Science* **325**, 1236–1239.

Koide, M., Soutar, A., Goldberg, E.D., 1972. Marine geochronology with ^{210}Pb. *Earth and Planetary Science Letters* **3**, 442–446.

Korsun, S., Hald, M., 1998. Modern benthic foraminifera off Novaya Zemlya tidewater glaciers, Russian Arctic. *Arctic and Alpine Research* **1**, 61–77.

Kossova, S.A., Dubinina, E.O., Miroshnikov, A.Yu., 2019. Mechanisms of seawater freshening in Tsivol'ki and Sedova Bays (Novaya Zemlya) according to isotope (δD, δ18O) data. In: *XXII Academician Vinogradov Symposium on the Geochemistry of Isotopes*. [In Russian.] GEOKhI RAN, Moscow, pp. 87–88.

Kotlyakov, V.M. (Ed.), 1978. *Katalog lednikov SSSR. Tom 3, Severnyj Kraj. Chast' 2, Novaja Zemlja* [Catalogue of glaciers USSR. Volume 3, Northern area. Part 2, Novaya Zemlya]. Hydrometeoizdat, Leningrad.

Kuptsov, V.M., 1986. *Absolyutnaya geokhronologiya donnykh osadkov okeanov I morei* [Absolute geochronology of oceanic and marine bottom sediments]. Nauka, Moscow.

Lambeck, K., Rouby, H., Purcell, A., Sun, Y., Sambridge M., 2014. Sea level and global ice volumes from the Last Glacial Maximum to the Holocene. *Proceedings of the National Academy of Sciences USA* **43**, 15296–15303.

Linderholm, H.W., Nicolle, M., Francus, P., Gajewski, K., Helama, S., Korhola, A., Solomina, O., et al., 2018. Arctic hydroclimate variability during the last 2000 years: current understanding and research challenges. *Climate of the Past* **14**, 473–514.

Lopatin B.G. (Ed.), 1999. *Gosudarstvennaya geologicheskaya karta Rossiiskoi Federatsii* [State geological map of the Russian Federation]. S-38-40. 1:1,000,000. Cartographic Production VSEGEI, St. Petersburg.

Luoto, T.P., Helama, S., 2010. Paleoclimatological and paleolimnological records from fossil midges and tree-rings: the role of the North Atlantic Oscillation in eastern Finland through the Medieval Climate Anomaly and Little Ice Age. *Quaternary Science Reviews* **29**, 2411–2423.

Luoto, T.P., Nevalainen, L., 2015. Late Holocene precipitation and temperature changes in Northern Europe linked with North Atlantic forcing. *Climate Research* **66**, 37–48.

Majewski, W., Szczuciński, W., Zajączkowski, M., 2009. Interactions of Arctic and Atlantic water-masses and associated environmental changes during the last millennium, Hornsund. *Boreas* **38**, 529–544.

Mangerud, J., Landvik, J.Y., 2007. Younger Dryas cirque glaciers in western Spitsbergen: smaller than during the Little Ice Age. *Boreas* **36**, 278–285.

Matthews, J.A., Briffa, K.R., 2005. The "Little Ice Age": re-evaluation of an evolving concept. *Geografiska Annaler, Series A: Physical Geography* **87A**, 17–36.

Matusevich, N.N., Sokolov, A.V., 1927. *Novaya Zemlya* [Novaya Zemlya]. Severnyi Pechatnik, Vologda, Russia.

Meeker, L.D., Mayewski, P.A., 2002. A 1400-year high-resolution record of atmospheric circulation over the North Atlantic and Asia. *The Holocene* **12**, 257–266.

Meier, M.F., Post, A., 1969. What are glacier surges? *Canadian Journal of Earth Sciences* **6**, 807–817.

Meire, L., Mortensen, J., Meire, P., Juul-Pedersen, T., Sejr, M.K., Rysgaard, S., Nygaard, R., Huybrechts, P., Meysman, F.J.R., 2017. Marine-terminating glaciers sustain high productivity in Greenland fjords. *Global Change Biology* **23**, 5344–5357.

Melkonian, A.K., Willis, M.J., Pritchard, M.E., Stewart, A.J., 2016. Recent changes in glacier velocities and thinning at Novaya Zemlya. *Remote Sensing of Environment* **174**, 244–257.

Miller, G.H., Brigham-Grette, J., Alley, R.B., Anderson, L., Bauch, H.A., Douglas, M.S.V., Edwards, M.E., et al., 2010. Temperature and precipitation history in the Arctic. *Quaternary Science Reviews* **29**, 1679–1715.

Mix, A.C., Bard, E., Schneider, R., 2001. Environmental processes of the ice age: land, oceans, glaciers (EPILOG). *Quaternary Science Reviews* **20**, 627–657.

Moore, D.M., Reynolds, R.C.J., 1997. *X-Ray Diffraction and the Identification and Analysis of Clay Minerals*. Oxford University Press, Oxford.

Moore, G.W.K., 2013. The Novaya Zemlya Bora and its impact on Barents Sea air-sea interaction. *Geophysical Research Letters* **40**, 3462–3467.

Murdmaa, I., Polyak, L., Ivanova, E., Khromova, N., 2004. Paleoenvironments in Russkaya Gavan' Fjord (NW Novaya Zemlya, Barents Sea) during the last millennium. *Palaeogeography, Palaeoclimatology, Palaeoecology* **209**, 141–154.

Nesje, A., Dahl, S.O., 2003. The "Little Ice Age"—only temperature? *The Holocene* **13**, 139–145.

Nesje, A., Dahl, S.O., Thun, T., Nordli, O., 2008. The "Little Ice Age" glacial expansion in western Scandinavia: summer temperature or winter precipitation? *Climate Dynamics* **30**, 789–801.

Nicolle, M., Debret, M., Massei, N., Colin, C., de Vernal, A., Divine, D., Werner, J.P., Hormes, A., Korhola, A., Linderholm, H.W., 2018. Climate variability in the subarctic area for the last 2 millennia. *Climate in the Past* **14**, 101–116.

Ó Cofaigh, C., Dowdeswell, J.A., 2001. Laminated sediments in glacimarine environments: diagnostic criteria for their interpretation. *Quaternary Science Reviews* **20**, 1411–1436.

Opel, T., Fritzsche, D., Meyer, H., 2013. Eurasian Arctic climate over the past millennium as recorded in the Akademii Nauk ice core (Severnaya Zemlya). *Climate in the Past* **9**, 2379–2389.

Ottesen, D., Dowdeswell, J.A., 2006. Assemblages of submarine landforms produced by tidewater glaciers in Svalbard. *Journal of Geophysical Research* **111**(F1), F01016.

Ottesen, D., Dowdeswell, J.A., Benn, D., Kristensen, L., Kristensen, H., Kristensen, O., Hansen, L., Lebesbye, E., Forwick, M., Vorren, T.O., 2008. Submarine landforms characteristic of glacier surges in two Spitsbergen fjords. *Quaternary Science Reviews* **27**, 1583–1599.

PAGES 2k Consortium, 2013. Continental-scale temperature variability during the past two millennia. *Nature Geoscience* **6**, 339–346.

Patton, H., Andreassen, K., Bjarnadóttir, L.R., Dowdeswell, J.A., Winsborrow, M.C.M., Noormets, R., Polyak, L., Auriac, A., Hubbard, A., 2015. Geophysical constraints on the dynamics and retreat of the Barents Sea ice sheet as a paleobenchmark for models of marine ice sheet deglaciation. *Reviews of Geophysics* **53**, 1051–1098.

Pawłowska, J., Zajączkowski, M., Łącka, M., Lejzerowicz, F., Esling, P., Pawlowski, J., 2016. Palaeoceanographic changes in Hornsund Fjord (Spitsbergen, Svalbard) over the last millennium: new insights from ancient DNA. *Climate in the Past* **12**, 1459–1472.

Petelin, V.P., 1967. *Granulometricheskiy analiz morskikh donnikh osadkov* [Grain-size analysis of the marine bottom sediments]. Nauka, Moscow.

Polyak, L., Forman, S.L., Herlihy, F.A., Ivanov, G., Krinitsky, P., 1997. Late Weichselian deglacial history of the Svytaya (Saint) Anna Trough, northern Kara Sea, Arctic Russia. *Marine Geology* **143**, 169–188.

Polyak, L., Gataullin, V., Okuneva, O., Stelle, V., 2000. New constraints on the limits of the Barents-Kara ice sheet during the Last Glacial Maximum based on borehole stratigraphy from the Pechora Sea. *Geology* **28**, 611–614.

Polyak, L., Lehman, S.J., Gataullin, V., Jull, A.J.T., 1995. Two-step deglaciation of the southeastern Barents Sea. *Geology* **23**, 567–571.

Polyak, L., Murdmaa, I., Ivanova, E., 2004. A high-resolution, 800-year glaciomarine record from Russkaya Gavan, a Novaya Zemlya fjord, eastern Barents Sea. *The Holocene* **4**, 638–644.

Polyak, L., Solheim, A., 1994. Late- and postglacial environments in the northern Barents Sea west of Franz Josef Land. *Polar Research* **13**, 197–207.

Polyakov, I.V., Pnyushkov, A.V., Alkire, M.B., Ashik, I.M., Baumann, T.M., Carmack, E.C., Goszczko, I., et al., 2017. Greater role for Atlantic inflows on sea-ice loss in the Eurasian Basin of the Arctic Ocean. *Science* **356**, 285–291.

Post, J.E., Bish, D.L., 1989. Rietveld refinement of crystal structures using powder X-ray diffraction data in Modern powder diffraction. In: Bish, D.L., Post, J.E. (Eds.), *Reviews in Mineralogy*. Walter de Gruyter, Berlin, pp. 227–308.

Prothero, D.R., Schwab, F., 2013. *Sedimentary Geology: An Introduction to Sedimentary Rocks and Stratigraphy*. 3rd ed. Freeman, New York.

Rusakov, V.Yu., Kuz'mina, T.G., Levitan, M.A., Toropchenova, E.S., Zhilkina, A.V., 2017. Lithology and geochemistry typification of surface sea-bottom sediment at the Kara Sea. *Oceanology* **57**, 214–226.

Rusakov, V.Yu., Kuz'mina, T.G., Toropchenova, E.S., Zhilkina A.V., 2018. Modern sedimentation in the Kara Sea: evidence from the lithological–geochemical investigation of surface bottom sediments. *Geochemistry International* **56**, 1076–1096.

Sapozhnikov, Yu.A., Aliev, R.A., Kalmykov, S.N., 2006. *Radioaktivnost' okruzhayushchei sredy. Teoriya I praktika* [Environmental radioactivity. Theory and practice]. BINOM Laboratoriya znanii, Moscow.

Serreze, M.C., Stroeve, J., 2015. Arctic sea ice trends, variability and implications for seasonal ice forecasting. *Philosophical Transactions of the Royal Society A: Mathematical Physical and Engineering Sciences* **373**, 20140159.

Shumskii, P.A., 1949. Sovremennoe oledenenie Sovetskoi Arktiki [Modern glaciation of the Soviet Arctic]. In: Saks, V.N. (Ed.), *Proceedings of AARI*, Vol. 11. Izd. Glavsevmorputi, Leningrad.

Spielhagen, R.F., Werner, K., Sørensen, S.A., Zamelczyk, K., Kandiano, E., Budeus, G., Husum, K., Marchitto, T.M., Hald, M., 2011. Enhanced modern heat transfer to the Arctic by warm Atlantic water. *Science* **331**, 450–453.

Svendsen, J.I., Alexanderson, H., Astakhov, V.I., Demidov, I., Dowdeswell, J.A., Funder, S., Gataullin, V., et al., 2004. Late Quaternary ice sheet history of eastern Eurasia. *Quaternary Science Reviews* **23**, 1229–1271.

Syvitski, J.P.M., 1989. On the deposition of sediment within glacier-influenced fjords: oceanographic controls. *Marine Geology* **85**, 301–329.

Taylor, S.R., McLennan, S.M., 1985. *The Continental Crust: Its Composition and Evolution*. Blackwell, Oxford.

Thouret, J.-C., Davila, J., Eissen, J.-P., 1999. Largest explosive eruption in historical times in the Andes at Huaynaputina volcano, a.d. 1600, southern Peru. *Geology* **27**, 435–438.

Trouet, V., Esper, J., Graham, N.E., Baker, A., Scourse, J.D., Frank, D.C., 2009. Persistent positive North Atlantic Oscillation mode dominated the Medieval Climate Anomaly. *Science* **324**, 78–80.

Trouet, V., Scourse, J.D., Raible, C.C., 2012. North Atlantic storminess and Atlantic Meridional Overturning Circulation during the last millennium: reconciling contradictory proxy records of NAO variability. *Global and Planetary Change* **84–85**, 48–55.

Udalov, A.A., Vedenin, A.A., Chava, A.I., Shchuka, S.A., 2019. Benthic fauna of Oga Bay (Novaya Zemlya, Kara Sea). *Oceanology* **59**(6), 931–940.

Verosub, K.L., Lippman, J., 2008. Global impacts of the 1600 eruption of Peru's Huaynaputina volcano. *EOS* **89**, 141–148.

Werner, J.P., Divine, D.V., Ljungqvist, F.C., Nilsen, T., Francus, P., 2018. Spatio-temporal variability of Arctic summer temperatures over the past 2 millennia. *Climate in the Past* **14**, 527–557.

Witze, A., 2008. The volcano that changed the world. *Nature*. https://doi.org/10.1038/news.2008.747.

Yokoyama, Y., Lambeck, K., De Deckker, P., Johnston, P., Fifield, L.K., 2000. Timing of the Last Glacial Maximum from observed sea-level minima. *Nature* **406**, 713–716.

Zeeberg, J., Forman, S.L., 2001. Changes in glacier extent on north Novaya Zemlya in the twentieth century. *The Holocene* **2**, 161–175.

Zeeberg, J., Lubinski, D.J., Forman, S.L., 2001. Holocene relative sea-level history of Novaya Zemlya, Russia, and implications for Late Weichselian ice-sheet loading. *Quaternary Research* **56**, 218–230.